Title

A real-world application of lane-guidance technologies - Automated snowblower

Journal

IEEE Transactions on Intelligent Transportation Systems, 8(3)

ISSN

1524-9050

Authors

Tan, Han-Shue
Bu, Fanping
Bougler, Benedicte

Publication Date

2007-09-01

Peer reviewed

A Real-World Application of Lane-Guidance Technologies – Automated Snowblower

Han-Shue Tan, Fanping Bu, Bénédicte Bougler

***Abstract*— This paper describes the development process and the initial field test results of an automated snowblower, focusing on one of the more difficult snow removal operations: blowing snow off the freeway alongside a guardrail without the snowblower touching the guardrail. The development process includes transforming this highway winter maintenance operation into a control problem, modeling a snowblower, designing control algorithms, devising human machine interface, and equipping a 20-ton snowblower with sensors and an actuator. Specific challenges include modeling the low-speed tire-induced oscillation, designing high-gain automatic control on front wheels while keeping rear steering under driver control, and implementing such a system under practical limitations. A new dynamic deflection tire model is incorporated into a bicycle model to account for the additional lateral dynamics. A low-order controller was first generated based on the understanding of the specific control problem and then refined and tuned iteratively using Linear Matrix Inequality (LMI) optimization. The initial winter field tests were successfully conducted with embedded magnetic markers along guardrails installed on the shoulders of Interstate-80 in the Sierra Mountain region close to Donner Summit in California, USA, during the winter of 2005.**

***Index Terms*— Highway maintenance, snow removal, lane guidance, low-speed tire model, vehicle lateral control, linear matrix inequality (LMI) optimization, human machine interface**

I. Introduction

A snowblower, a.k.a. a rotary snowplow, is a massive snow removal apparatus that blows snow high into the air and off the roadway. It is a key component of the snow removal strategy employed by snow fighters, especially on highways that travel across mountains. To effectively remove the snow built up along the roadside created by either a single snowplow or a fleet of snowplows, the operator needs to drive the snowblower on the edge of the road and often with a very tight tolerance range in order to eliminate the left-over snow "bleeding" back into the highway. This method of driving becomes even more difficult when the snowblower is operated along a guardrail.

An operator generally uses the rear steering joystick to position the snowblower in the appropriate "crab" angle (Fig. 1) before he reaches a section of guardrail. Typically, the rear edge of the vehicle is about 0.1-0.8 of a meter further away from the edge of the road or guardrail than that of the front end of the blower. The operator then drives the huge vehicle body toward the guardrail until the front side of the blower's head touches it. He then "tries" to maintain a somewhat continuous contact between the blower's head and the guardrail using his hands (to feel the pressure), his ears (to hear the contact sounds), and his eyes (to look for snow poles and obstacles) as he plows forward. Since the blower's head can weigh up to 6 tons, it creates a natural oscillation when it hangs in front of the snowplow body. Consequently, the snowblower continuously "bounces" onto and off the guardrail. "Riding on the guardrail," as the operators commonly term it, creates damage such as tilting, ripping, and tearing of the guardrail, which is often serious enough that it can be easily identified by travelers passing by (see Fig. 2 for an example of a section of damaged guardrail). These damages lead to frequent repairs and replacements of guardrails in treacherous mountain regions. While guardrails require rehabilitation throughout all the areas maintained by the Department of Transportation, the frequency of rehabilitation due to snowblower damage, typically once every couple of years, represents a significant cost, and thus becomes an opportunity for a cost effective application of advanced lane-guidance technologies such as precision steering control. The application of precision steering control, if successful, will reduce, even eliminate contact between the snowblower and guardrail, while also improving the consistency and accuracy of the work performed. Furthermore, this application will increase operational safety by allowing the operator to concentrate on "plowing", and remove the exhausting necessity of "drive by feeling" as well as reduce the operator's visual fatigue, a major complaint during long-hour winter operations. Furthermore, limiting the damage to the guardrail also improves the safety of the traveling vehicles in the event of an emergency situation.

A project to develop a prototype automated snowblower to be used by the California Department of Transportation operators to perform real snow removal operations under harsh winter environments was initiated in 2000 [1]. Various lateral sensing and referencing technologies were available to provide lateral position for the precision steering control, and were researched for this application. For example, in [2, 3], video cameras are used to determine the vehicle position for guidance or for control. However, the vision based systems are generally more sensitive to the environmental factors such as lighting, weather, or pavement conditions; and the machine vision does not penetrate snow and ice that cover the lane markings. GPS is another way to determine vehicle position for the purposes of guidance or control with lower infrastructure cost [4, 5, 6]. However, the current GPS system does not provide sufficient reliability under possible multipath and blockage scenarios in the mountainous areas. In order to quickly demonstrate the feasibility of the automatic lane guidance concept, a magnetic marker-based sensing system [7,

8] was chosen for the initial implementation primarily because of its high reliability and accuracy (better than 1 cm) under all weather conditions [9]. The mountainous highway I-80 near Donner Summit, 30 km from Lake Tahoe, was chosen to be the first field test site. In 2001, magnets were installed along the guardrails of Interstate 80, at a 1.2 meter spacing and 4 feet away from the guardrail. Binary coding of the magnetic markers was designed (north pole up vs. south pole up) to provide two types of information about the guardrail: the guardrail location (right or left of the blower) and the end of guardrail. Eight sections of the guardrail were equipped with the magnets for the initial feasibility operations with a total length of 1.46 km between Soda Spring and Kingvale (at elevation of around 2000 meters). The automated snowblower was successfully tested during the winters of 2004 and 2005.

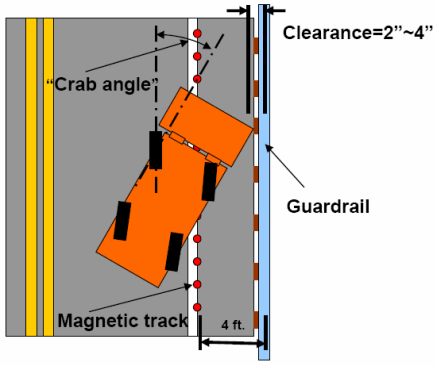

Fig. 1. Snowblower operation.

Fig. 2. A section of guardrail damaged by snowblower.

This paper describes the process of transforming this real-world application problem into system requirements, using various control techniques to address modeling and control issues, implementing a prototype system with human machine interface, and field testing under winter operational environment. The main objectives of the papers are to provide an overview of this particular control application as well as to point out several key design elements of the proposed solution. Those key elements include (1) the importance of the often-ignored low-speed tire oscillations, (2) the robustness of a specific position-and-angle feedback controller structure, and (3) the use of a simple LED display interfacing between the controller and the driver. This paper is organized as follows: Section II defines the problem and requirements; Section III describes the snowblower lateral dynamics using an enhanced bicycle model that includes a new dynamic deflection tire model to account for the tire induced low-speed oscillations; Section IV constructs a feedback control structure based on physical system insights and formulates the linear matrix inequality (LMI) optimization accordingly; hardware, software and HMI designs for the prototype system are illustrated in Section V; winter field test results are presented in Section VI; and Section VII concludes the paper.

II. Problem and Requirements

The initial "performance requirement" from the Maintenance department seemed to suggest it to be a difficult but straightforward project: controlling a snowblower to maintain a distance between 2 and 4 inches from the guardrail. An examination of the project objectives revealed that the success of the project would stem from positive responses to the following questions: (1) Does the system reduce or eliminate guardrail damage caused by the blower? (2) Does the system effectively support snow removal operations? (3) Does the operator like the system and would the operator use the system? As a result, the initial requirements for the automated snowblower system were defined as follows:

- "Track" accurately along guardrail (2 to 4 inches)
- Support various snow removal operations
- Survive harsh winter environments (snow, ice, salt, water, dirt, wind)
- Possess a simple operation procedure, tolerate operator mistakes, require only a small amount of training
- Low operator distractions
- Reliable and safe automated operation

During the first winter's ride-along observation in a snowblower, the researchers soon realized that accurately controlling a 6-ton oscillatory blower head on a 20-ton vehicle along the highway shoulder dotted with potholes while pushing and blowing snow and ice was not easy. To make things more difficult, the driver also, from time to time, has to adjust the rear steering angle to compensate for various cutting load and road curvature, move the head (also-called "box") position and tilt angle to account for different road curvatures and slopes, inclination and resistant force, as well as change the speed from stop to go to react for various road and snow conditions. The control system must allow the operator to engage the automation with ease and to switch off any time he wants. The system also needs to survive both the operator's intervention, either intentionally or unintentionally; and environmental disturbances, such as hitting a guardrail or running into an ice patch. Furthermore, during early perusals of the literature, we also discovered that little research work exists for this low-speed heavy vehicle tire induced oscillation. Nevertheless, the project goals dictated that these obstacles needed to be overcome. The system requirements were then modified to include the following additional specific items:

- Automatically compensate for the operator's rear steering action
- Maintain robustness against various blower head positions and the resultant front tire loading conditions
- Maintain robustness against rough and uneven road surface conditions, including potholes
- Provide sufficient control at any operational speeds including stop and go
- Allow on-demand operator transitions and interventions

Since the snowblower used for this study still performs normal winter snow removal operations, several design constraints were imposed based on the considerations in safety, operation and maintenance. First of all, the installation and application of any components to the snowblower, especially the steering actuator, should not affect normal manual operations, nor should it imperil or degrade the

performance of any existing vehicle components. Second, unless a rear steering sensor can survive the harsh winter exposure, it is not recommended. The rear wheel is actuated by open-loop hydraulic valves. The driver controls the rear steering using a "joy-stick" type controller with 7 LED's, each connected to a contact switch, indicating the rough location of the rear wheel angle. However, those switches or LED's are broken from time to time; operators often adjust the joy-stick (rear wheel angle) based on his experience, rear view from the side mirror, and feel. Obtaining precise position reading by measuring flow rates of hydraulic fluid and installing sensors on the linkages next to the rear wheel are both difficult. High-precision position sensors, such as rotary position encoder and linear transducer, are not encouraged to be mounted on the rear steering mechanism that is often encapsulated by ice. Finally, since the operator cuts in and out of the guardrail operation, the only reliable information that is available through the magnetic pattern is the indicator for left/right shoulder, and for the approaching of the "end of the magnets." Typical "preview" road information such as curvature or super-elevation will not be available to the controller.

Many critical tasks were performed under the above limitations and requirements. The snowblower dynamic was first verified using an enhanced bicycle model with a new flexible tire model to account for the additional lateral oscillation under low speed steering control. A feedback control structure was introduced based on the resultant model and the common control practices. The linear matrix inequality (LMI) optimization was used as a tool to validate the proposed control structure and to facilitate parameter tuning. Iterations and tuning concluded a simple control structure that achieved the desired control objectives under multiple control constraints. Hardware and software were developed, which included sensor instrumentation, signal processing coding, circuit design, actuator installation and servo controller design. Human machine interface (HMI) was developed and implemented based on operational analysis, operator feedback, and field tests. Safety-critical issues were designed and reviewed, covering subjects of interest that included robust control, fault detection, failure mode analysis, warning systems, and redundancy. Finally, various tests were conducted to evaluate and refine the system design. The following sections describe several of the critical tasks mentioned above.

III. MODELING

Most steering control algorithms are developed based on the bicycle model [10]. In the conventional bicycle model, the rear wheel is assumed to be fixed to the vehicle body. Lateral force is a linear static force which is proportional to the vehicle side slip angle. For the vehicle lateral dynamics, the tires are assumed to have deformations only in the lateral direction due to the vehicle side slip.

The conventional bicycle model, however, is not adequate in describing lateral behavior of a snowblower. A snowblower is a four-wheel-steering vehicle. Rear wheel steering is independent of the front wheel steering and is directly controlled by the operator. Secondly, a snowblower is a heavy-duty vehicle with about 20 tons' worth of weight. A 6-ton snowblower head is installed on the front of the vehicle. Such weight distribution creates large normal force on the front tires and "amplifies" the effects of the front tires' flexible torsion mode. As evident in the experimental data in Fig. 3, a resonant mode due to tire's flexibility shows up around 0.8Hz in the frequency response from steering angle to yaw rate, especially under low speeds. This phenomenon turns out to be the dominant low-speed dynamics of the snowblower; and it cannot be explained by the simple conventional bicycle model.

In order to capture the fundamental characteristic of the snowblower lateral dynamics and provide an accurate design model for the automatic steering controller design, an enhanced bicycle model, which incorporates rear wheel steering, tire flexible mode and various disturbances, is developed and verified with experimental data. Vehicle dynamics equations are derived using Newtonian method and the Dynamic Deflection Tire (DDT) model in [11]. A more detailed derivation process is explained in Appendix A.

When assuming small steering angles and constant vehicle speed v_r, the lateral dynamics of the snowblower with respect to the road reference frame can be expressed in the state space representation as in Eq. (1).

$$
\begin{bmatrix}
1 & 0 & 0 & 0 & 0 & 0 & 0 \\
0 & 1 & 0 & 0 & 0 & 0 & 0 \\
-2(D_{lat}^{f}+D_{lat}^{r}) & 0 & M & -2(D_{lat}^{f}l_1-D_{lat}^{r}l_2) & 0 & 0 & 0 \\
0 & 0 & 0 & 1 & 0 & 0 & 0 \\
0 & 0 & 0 & 0 & 1 & 0 & 0 \\
-(2D_{lat}^{f}l_1-2D_{lat}^{r}l_2) & 0 & 0 & -(2D_{lat}^{f}l_1^{2}+2D_{lat}^{r}l_2^{2}) & 0 & I & 0 \\
0 & 0 & 0 & 0 & 0 & 0 & 1
\end{bmatrix}
\begin{bmatrix}
\dot{y}_u \\ \dot{y}_s \\ \ddot{y}_s \\ \dot{\varepsilon}_u \\ \dot{\varepsilon}_s \\ \ddot{\varepsilon}_s \\ \dot{\delta}_{eff}^{f}
\end{bmatrix}
$$

$$
=
\begin{bmatrix}
A_{11} & A_{12} & 0 & 0 & A_{15} & 0 & A_{17} \\
0 & 0 & 1 & 0 & 0 & 0 & 0 \\
A_{31} & A_{32} & A_{33} & A_{34} & A_{35} & A_{36} & 0 \\
0 & 0 & 0 & A_{44} & A_{45} & 0 & A_{47} \\
0 & 0 & 0 & 0 & 0 & 1 & 0 \\
A_{61} & A_{62} & A_{63} & A_{64} & A_{65} & A_{66} & A_{67} \\
0 & 0 & 0 & 0 & 0 & 0 & A_{77}
\end{bmatrix}
\begin{bmatrix}
y_u \\ y_s \\ \dot{y}_s \\ \varepsilon_u \\ \varepsilon_s \\ \dot{\varepsilon}_s \\ \delta_{eff}
\end{bmatrix}
$$

$$
+
\begin{bmatrix}
0 \\ 0 \\ 0 \\ 0 \\ 0 \\ -k_2 \\ v_r/\sigma_{yaw}
\end{bmatrix}
\delta_f +
\begin{bmatrix}
v_r/(l_1+l_2) & 0 & 0 & 0 \\
0 & 0 & 0 & 0 \\
0 & -Mv_r^{2} & 1 & 0 \\
-v_r/(l_1+l_2) & v_r & 0 & 0 \\
0 & 0 & 0 & 0 \\
0 & 0 & 0 & 1 \\
0 & 0 & 0 & 0
\end{bmatrix}
\begin{bmatrix}
\delta_r \\ \rho \\ F_d \\ M_d
\end{bmatrix}
\qquad (1)
$$

where $A_{11}=-v_r/\sigma_{lat}$, $A_{12}=v_r/\sigma_{lat}$, $A_{15}=v_r$, $A_{17}=l_2v_r/(l_1+l_2)$,
$A_{31}=2(C_{lat}^{f}+C_{lat}^{r})$, $A_{32}=-2(C_{lat}^{f}+C_{lat}^{r})$, $A_{33}=-2(D_{lat}^{f}+D_{lat}^{r})$,
$A_{34}=2(C_{lat}^{f}l_1-C_{lat}^{r}l_2)$, $A_{35}=-2(C_{lat}^{f}l_1-C_{lat}^{r}l_2)$,
$A_{36}=-2(D_{lat}^{f}l_1-D_{lat}^{r}l_2)$, $A_{44}=-v_r/\sigma_{lat}$, $A_{47}=v_r/(l_1+l_2)$,
$A_{61}=2(C_{lat}^{f}l_1-C_{lat}^{r}l_2)$, $A_{62}=-2(C_{lat}^{f}l_1-C_{lat}^{r}l_2)$,
$A_{63}=-2(D_{lat}^{f}l_1-D_{lat}^{r}l_2)$, $A_{64}=2(C_{lat}^{f}l_1^{2}+C_{lat}^{r}l_2^{2})$,
$A_{65}=-2(C_{lat}^{f}l_1^{2}+C_{lat}^{r}l_2^{2})$, $A_{66}=-(D_{lat}^{f}l_1^{2}+D_{lat}^{r}l_2^{2})$, $A_{67}=k_2$
$A_{77}=-v_r/\sigma_{yaw}$.

The state vector $x=[y_u, y_s, \dot{y}_s, \varepsilon_u, \varepsilon_s, \dot{\varepsilon}_s, \delta_{eff}^{f}]^T$ includes: y_u, ε_u, the tire contact patch position and angle as defined in Appendix A; δ_{eff}^{f}, the effective front steering angle as defined also in Appendix A; y_s, $\dot{y}_s$, the vehicle lateral displacement

and its derivative at CG w.r.t. road reference frame; and $\varepsilon_s, \dot{\varepsilon}_s$, the vehicle yaw angle and its derivative w.r.t. road reference frame. The control input is the front steering angle δ_f. The disturbances are: ρ, the road curvature; δ_r, rear steering angle; F_d, the disturbance force at CG along the lateral direction; and M_d, the disturbance torque about yaw axis. Disturbances from snow blowing operation, different road surface conditions due to snow and ice distributions and unevenness of road surface at the shoulder are hard to model. Their effects are lumped into F_d and M_d. The sensor measurements are speed v_r; lateral displacement y_s (measured by front and rear magnetometers); and vehicle yaw angle ε_s (computed by the measurements from the front and rear magnetometers and yaw rate). Table 1 lists the variables and parameters that were identified from the test data.

Fig. 3 shows the comparisons among the conventional bicycle model, the enhanced bicycle model and the experimental data. The enhanced bicycle model matches the experimental data especially on the resonant peak around 0.8Hz. It is worthwhile noticing that this particular resonant mode is more prominent at low speeds, exhibiting the same characteristics as those observed and recorded during the snowblower test drives. This additional resonant mode is also the key control obstacle that needs to be overcome.

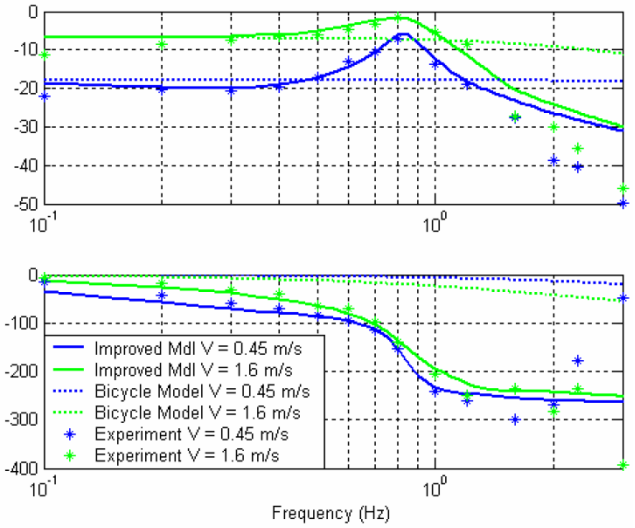

Fig. 3. Bode plot from front steering angle to yaw rate.

Table 1 Identified parameters for Snowblower

M (kg)	20,500	σ_{yaw} (m)	0.45	D_{lat}^f (Ns/m)	9,000
I(kgm^2)	168,250	σ_{lat} (m)	1.0	D_{lat}^r (Ns/m)	9,000
l_1(m)	1.3	C_{lat}^f (N/m)	350,000	k_2 (Nm)	500,000
l_2(m)	2.2	C_{lat}^r (N/m)	350,000		

IV. Controller Design

This section describes the evolution process of how the automatic steering controller was developed. The process roughly consists of the following three steps. A sketch of the controller structure was generated based on the engineering understanding of this particular control problem. Several control syntheses were then used to validate such a controller structure. This paper presents the LMI optimization approach because it was also used as a tool for refining the controller as well as supporting the parameter tuning. Finally, with design and test iterations, a low-order controller was constructed from the resultant synthesized controller. The associated physical meaning of the low order controller parameters facilitates the tuning process in the field.

The objective of the automated snowblower steering controller is to keep the lateral error at the head of the snowblower, $y_h = y_s + l_3\varepsilon_s$, small by using the front steering angle δ_f as the control input, where l_3 is the distance between blower head and CG. There are several difficulties inherent in the design of this controller. First, the heavy blower head creates a large normal force on front tires and thus amplifies the front-tire flexible torsion mode. As a consequence, the blower head tends to oscillate in response to the steering input. The enhanced bicycle model helps capture the additional flexible torsion motion; however, to mitigate its effects and keep the lateral error small, a low-frequency high-gain feedback of the lateral displacement at the blower head is likely an important component of the controller.

Secondly, since installing reliable and accurate sensors that measure the driver's rear steering actuation under the current project phase is neither economical nor practical; the rear steering is treated as a major source of disturbance. By examining Fig. 1, one can observe that, $\delta_f \cong \delta_r \cong -\varepsilon_s$ under the steady state condition when the snowblower is crabbing along the guardrail. This observation implies that $-\varepsilon_s$ is likely to be another critical component of the steering command to attenuate disturbance from the rear steering action. This "negative vehicle angle" feedback has the potential to (1) reduce the steady-state error, (2) speed up the transient response, and (3) increase the closed-loop damping (similar to that shown in the "look-ahead" control scheme [7]).

Thirdly, the system is subject to multiple uncertainties (such as changes in road surface conditions), large external disturbances from curvature change, and external loads from blowing and pushing snow and ice. These external loads are represented by the lumped disturbances F_d and M_d.

Consequently, the vehicle angle $-\varepsilon_s$ and the lateral head displacements y_h are chosen as the plausible inputs to the steering controller. The resultant controller structure is $\delta_f = G_\varepsilon(s)(-\varepsilon_s) + G_y(s)(y_h)$. Both $G_\varepsilon(s)$ and $G_y(s)$ is likely to consist of a low-pass filter responsible for rolling off high frequency noises (above ~1Hz) and a "notch-type" filter with a notch frequency of about 0.8Hz to suppress the flexible torsion mode. In addition, the steady state gain for $-\varepsilon_s$ should be close to 1 and large for y_h. As a result, the control structure can be further broken down as follows:

$$\delta_f = G_{rolloff}(s)G_{notch}(s)(-\varepsilon_s + G_{highgain}(s)y_h), \quad (2)$$

where $G_{rolloff}(s)$ is a low-pass filter; $G_{notch}(s)$ a "notch-type" filter, and $G_{highgain}(s)$ a low-frequency high-gain compensator that may include some form of an integrator.

Various control techniques can be employed to design the feedback controller; we choose the mixed H_2/H_∞ synthesis for both performance and robustness. The generalized H_2 norm is a convenient way to express performance requirements such as disturbance rejection of the snowblower operation. Since the generalized H_2 norm represents the system gain from L_2 to L_∞, its value can be interpreted as the worst time-domain amplification of the disturbance input with finite energy [12]. In addition, the H_∞ criterion provides a natural expression for the system robustness.

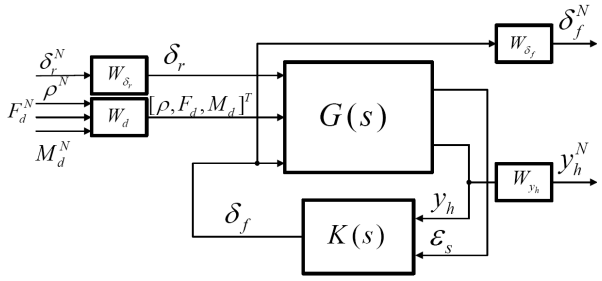

Fig. 4. Block diagram of control loop.

The mixed H_2/H_∞ synthesis can be formulated as shown in Fig. 4, where $G(s)$ represents the open-loop snowblower lateral dynamics and $K(s)$ represents the controller to be synthesized. W_d, W_{δ_r}, W_{δ_f} and W_{y_h} are the control design weighting functions. By denoting:

$$y_h^N = T_1(s)(\delta_r^N, \rho^N, F_d^N, M_d^N)^T ; \delta_f^N = T_2(s)(\delta_r^N, \rho^N, F_d^N, M_d^N)^T \quad (3)$$

where T_1 and T_2 are the transfer functions from the disturbance to the snowblower head lateral deviation and to the front steering control, respectively. Minimizing the H_2 norm of T_1 imposes the performance requirement described above. Minimizing H_∞ norm of T_2 increases the system robustness against unstructured additive uncertainties. Since T_1 and T_2 represent two channels with different roles in the control design, it is desirable that these two channels are treated separately. In the traditional H_2 or H_∞ design, these two channels are usually combined together with different weighting functions and can be optimized only for either H_2 or H_∞ norm. In [12], a LMI-based multi-objective strategy is proposed to treat each channel separately with different norm criteria. Such design technique provides more design flexibility compared with traditional design and is therefore adopted for the control validation and design in this paper.

The control objective is to minimize $\|T_1(s)\|_2$ subjected to $\|T_2(s)\|_\infty < \gamma$. This can be interpreted as maximizing system disturbance rejection performance with guaranteed system robustness against unstructured additive uncertainties. Such mixed H_2/H_∞ synthesis problem can be solved via LMI optimization [13, 14]. A critical design issue in the mixed H_2/H_∞ synthesis problem is the selection of the weighting functions. The relevant design parameters and weighting functions are explained as follows:

- $\gamma = 1.2$: Field tuning revealed that $\gamma = 1.2$ is a suitable value for this application. The constraint means that the robustness margin guaranteed by the controller is 1/1.2=0.83.
- $W_{y_h} = \dfrac{s+0.1\pi}{2(s+0.04\pi)}$: Due to the relatively slow vehicle lateral dynamics, the snowblower will not react to the high frequency content of the lateral error. The penalty on the lateral deviation is set high on low frequency.
- $W_{\delta_f} = \dfrac{200000s^2 + 4398200s + 4934800}{s^2 + 439.823s + 98696}$: The closed-loop band-width of the steering actuator is limited to 5 Hz for command amplitude under 20 degrees (steering wheel) and 2.5 Hz for command amplitude between 20 and 60 degrees. The weight on the control input is designed to penalize high frequency control effort to avoid chattering and saturation. The weight penalty starts to increase from 0.25 Hz and levels out at 50Hz.
- $W_d = diag[\dfrac{3\times10^{-5}s^2 + 0.0029s + 0.132}{s^2 + 8.8s + 39}, \dfrac{13s^2 + 1172s + 52637}{s^2 + 8.8s + 39}, \dfrac{20s^2 + 1759s + 78956}{s^2 + 8.8s + 39}]$: Highway road curvature usually changes slowly. Although other disturbance force or torque could contain high frequency content, the snowblower will not respond to the high frequency component because of its slow lateral dynamics. Therefore, the disturbances are modeled as low-pass filters with 1 Hz cornering frequency, which are faster than the dominant snowblower dynamics.

As an example of the controller, the dashed lines in Fig. 5 and 6 show the frequency responses of the synthesized controller at $v_r = 1m/s$. The solid lines in Fig. 5 and 6 plot the two relative low-order controllers (4th for ε_s to δ_f; and 6th for y_h to δ_f) that match the synthesized controllers at the same speed. As shown in Fig. 6, the steering angle input is always in the opposite direction (i.e., $\delta_f = -\varepsilon_s$) of the vehicle angle at low frequency. As predicted, this negative vehicle angle feedback is the key component that not only creates counter steering against the static-state rear steering disturbance, but also provides a damping effect that increases the phase margin of the closed loop system. By using the initial controller structure in Eq. (2) as a starting point, and examining the synthesized controllers at different speeds, the following relatively low-order controller structure is proposed:

$$\delta_f = G_{cl}(s)(-G_{c\varepsilon}(s)\varepsilon_s + G_{cy}(s)y_h), \quad (4)$$

where $G_{cl}(s)$ is a low-pass filter that removes unwanted high frequency control behaviors; $G_{c\varepsilon}(s)$ is a lag-lead compensator for the "negative" vehicle angle feedback; and $G_{cy}(s)$ is an "integrator" plus a lag-lead compensator for the blower head position feedback. The associated meanings of the corresponding control parameters facilitate the tuning process. The matched "low-order" controllers in Fig. 5 and 6, as were implemented in the final design, are listed below:

$$G_{cl}(s) = \frac{6.911^2(s+43.982)}{43.982(s^2 + 2*0.55*6.911s + 6.911^2)} \quad (5.1)$$

$$G_{c\varepsilon}(s) = 0.73\frac{43.982}{(s+43.982)}\frac{2.3876^2(s^2 + 2*0.18*5.0265s + 5.0265^2)}{5.0265^2(s^2 + 2*0.42*2.3876s + 2.3876^2)} \quad (5.2)$$

$$G_{cy}(s) = 0.1\frac{(s+0.9425)(s+0.06283)}{s^2} \frac{2.3876^2(s^2+2*0.18*6.2832s+6.2832^2)}{6.2832^2(s^2+2*0.42*2.3876s+2.3876^2)} \quad (5.3)$$

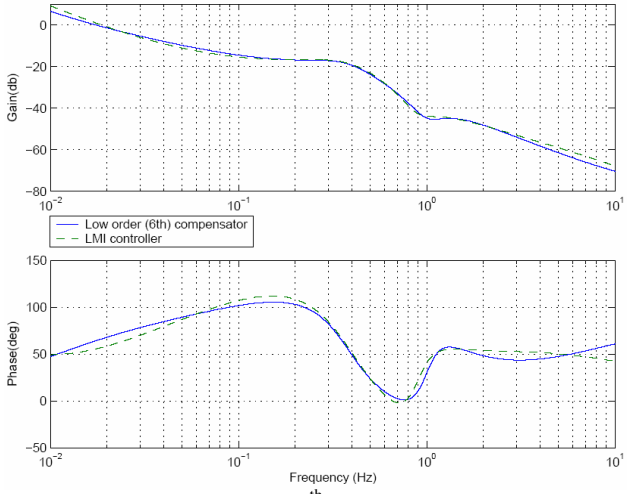

Fig. 5. Synthesized and matched 6th order controller TF's from lateral deviation at blower head to steering angle ($v_r = 1m/s$).

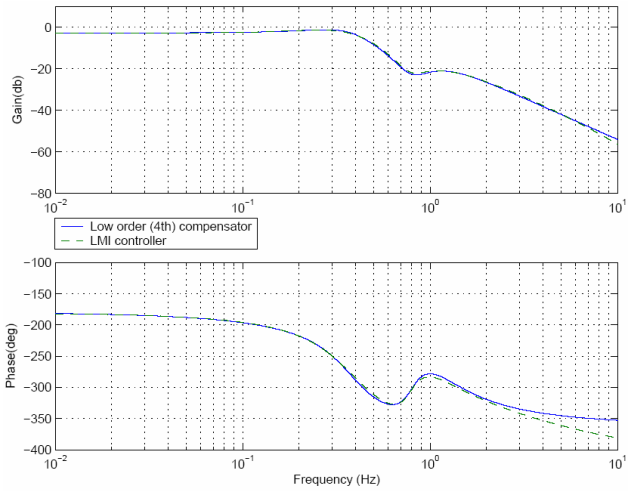

Fig. 6. Synthesized and matched 4th order controller TF's from vehicle yaw angle to steering angle ($v_r = 1m/s$).

Although the controllers in Eq. (5) do not look exactly the same as those suggested by Eq. (2), one will realize that Eq. (5) does contain all key components specified by the proposed structure in (2) by comparing them carefully. The second part of Eq. (5.2) is an "unbalanced" notch filter with the "notch" frequency of 0.8Hz (pole pair at 0.38Hz with damping ratio 0.42, zero pair at 0.8Hz with damping ratio 0.18). A similar "unbalanced" notch filter is also found with the "notch" frequency of 1Hz in Eq. (5.3). These two unbalanced "notch" filters perform the functions of $G_{notch}(s)$ in Eq. (2). The first part of Eq. (5.2) increases the roll-off order of $G_{rolloff}(s)$ for the negative vehicle angle feedback. Finally, the first part of Eq. (5.3), a low-frequency high-gain compensator based on a "double" integrator, is $G_{highgain}(s)$ in Eq. (2).

In practice, snowblower lateral dynamics can be regarded as a linear parameter-varying system with respect to the vehicle speed v_r. Due to the large mass and slow operating speeds, the speed variations during operation are generally small. A practical approach for the synthesis is to design the controller at several speed grid points (at 0.5, 1.0, 2.0 and 4.0 m/s for this case) and use interpolation for implementation. Iterations among applying the control syntheses, transforming into a low-order controller, and tuning the low-order controller in the field resulted in successful winter field tests along the shoulders of Interstate-80.

V. Prototype System Design

The automated steering control system had to be designed to operate under harsh winter conditions and be subject to extreme external disturbances. The design of this automated system includes iterations of "methodology" and "synthesis". It is a continuous evolution of the following design elements: problem definition, requirement specification, system configuration, hardware installation, software architecture, control algorithms, human machine interface, fault detection and management, and testing and evaluation.

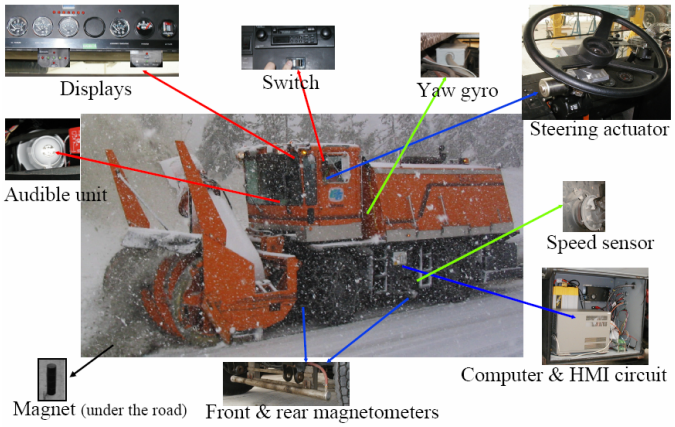

Fig. 7. Prototype components of the automated Snowblower.

The first prototype automated control was an "add-on" system with the following components installed on a conventional Kodiak Northwest single engine rotary snowplow with full hydrostatics as shown in Fig. 7. A computer with a data acquisition unit that processed information and determined control and guidance actions was the "brain" of the system. The lateral positioning system consisted of two sets of magnetometers, one underneath the front axle, and the other one mounted in between the front and rear wheels, which measured the field strength of magnetic markers installed under the roadway. A DC motor attached to the steering column with angular sensors was the steering actuator. A yaw gyro and an axle speed sensor measuring vehicle yaw rate and speed were used as the supplementary sensors during extremely low speed operations. Finally, a Human Machine Interface (HMI) unit, consisting of the local electronic circuit, a toggle switch, LED displays and an audible device, interfaced with the operator for essential information and commands for automation.

The key software components that collectively constitute the necessary intelligence of the automated system are: a signal processing algorithm that provides consistent location estimates; a steering servo that carries out the steering command under highly nonlinear mechanical characteristics and unpredictable disturbances; a high-gain "lane-keeping" controller that accurately follows the "magnets" without preview information; adaptive exception controls that can cope with "abnormal" scenarios; a "transition" controller that executes "on-demand" transitions between automated and manual control; a simple HMI that facilitates clear operator state awareness and prompts timely responses under both normal and emergency scenarios; as well as a fault detection and management system that detects system irregularities and provides a warning and conducts preventive actions.

Fig. 8. Status LED of HMI.

The effectiveness of the design is evident in the HMI system. It consists of the following four elements: a transition toggle switch which allows the operator to switch the system on and off; the status LED's which displays the system's current status; the guidance LED's which displays the position of the tip of the blower head with respect to the guardrail; and an audible unit that produces the following three different sounds: acknowledgment (transition to auto steering), end of magnets (approaching end of guardrail), and emergency (take control now). The core of this HMI is made up of four status LED's (as shown in Fig. 8): GREEN when the system is ready for transition; WHITE when it is under driver's control; BLUE when it is under automated control; and RED when there is a problem. It identifies the four key pieces of information for automation: system on or off, readiness for transitioning to automation, current state of automation, and the presence of a fault. The operator simply approaches the guardrail the same way as he or she always does. A separate supportive guidance LED displays the current "tip location" of the blower head. Once the blower is within its acceptable crab angle range, the system is ready to transition to automation, and the GREEN LED will be lit. Once the GREEN status LED is on, the driver can switch to automated control any time he wishes by pushing down the AUTO switch. With a soft acknowledgement sound, the BLUE status LED will then be lit, indicating the blower is transitioned to automated steering control. The operator can resume manual control by pushing the MANUAL switch or by overriding the steering wheel at any time. The flashing RED LED, with the emergency sound beeping, signals the driver to take over control immediately.

VI. Field Tests

Three types of field tests were conducted:

Simulated guardrail tests: A section of simulated guardrail was set up using traffic cones along a segregated test track with embedded magnets inside the Kingvale maintenance yard. The test scenarios included: left/right guardrail tracking, different crab angle tracking, different blower head (box) position and chute orientation, speeds from stop to 9 mph, various initial transitioning conditions, and various emergency shut off situations. This method provided an effective and safe environment for the system's development as well as for the initial operator training and feedback.

Initial road tests: Tests were first conducted along the Interstate-80 highway under fair weather conditions on ground free of snow where operators performed snow removal functions as normal operations. These tests provided an opportunity for the researcher to refine the system according to the operator feedback and the data analysis.

Winter operational field tests: Two initial field tests were conducted along the guardrails of the Interstate-80 under real winter operational conditions: the first one with light snow conditions (3/4/2005), and the second one under a heavy winter storm, blowing accumulated wet snow (3/22/2005).

Fig. 9. Field test (blowing wet snow during a winter storm).

Five operators have operated the automated snowblower. Since the field tests were conducted during the busy winter operation period, any available operators were used. Several operators had very limited training in the automated snowblower prior to the tests. A typical test procedure for a new operator was as follows:

1. the researcher conducted a 10-15 minute short description of the system in the maintenance yard
2. the driver practiced pushing the switches for turning the automated control off and on a few times
3. the operator performed normal snow removal operations once he left the yard
4. the operator pushed the switch for automated control as instructed by the ride-along researcher for the first guardrail when the 'ready" light was on
5. the operator switched off automated control when the "end of magnets" noise sounded, as instructed by the ride-along researcher for the first guardrail
6. the operator switched on and off as suggested by the automated system starting from the second guardrail if he felt comfortable in doing so
7. the researcher conducted a short operator interview and the operator filled in a human factor questionnaire

Data from two different trial days with two different test conditions are presented in this paper. They were from (a)

good weather with no snow on the ground on 2/3/2005; and (b) stormy weather with heavy wet snow on the ground on 3/22/2005 (as shown in Fig. 9). It is worthwhile noticing that Fig. 9 also shows a faint trace of the guardrail after the automated snowblower has passed; and it indicates the closeness of the blower head to the guardrail.

Figs. 10-11 present plots from the data saved during these test runs. Fig. 10 shows an automated test run along right guardrail #1 on I-80 with no snow on the ground on Feb. 3, 2005. The driver changed the crab angle from -3 degrees to -1 degrees, and changed speed from 2 mph to 4 mph. It can be observed that the head of the snowblower tracks very well along the right guardrail (located at 20 cm in this figure) and almost never touches it (such contact, should it happened, was never observed or felt). The standard deviation of the tracking error under automation is 3.3 centimeters.

Fig. 11 shows an automated test run also along right guardrail #1 during a severe late winter storm that lasted two days. The test was conducted on March 22, 2005, after a significant amount of wet snow had already accumulated on the ground. The driver kept an almost constant crab angle (~-4 degrees); with speed ranging from 2 mph to 3 mph. According to the operator, the load of snow-cutting was heavier than in a normal operation for this particular test run because he operated at a speed slightly higher than what he normally would do under the same condition. It can be observed that the head of the snowblower still tracked very well along the right guardrail. Although a few locations in Fig. 11 have shown possible slight brushing against the guardrail, no contact was felt by the operator during operation (these positions "overshoots" may have been caused by the amplification of the measurement noise in computing the blower head location). The standard deviation of the tracking error under automation was 4.1 centimeters. By comparing Fig. 11 and Fig. 10, it can be observed that the standard deviation of the tracking error increased from 3.3 centimeters to 4.1 centimeters when blowing wet and heavy snow.

The general observations and conclusions from the initial tests are:

1. The system performed the automated steering function as designed along the guardrail.
2. The operators learned to use the system quite easily; they generally had very favorable impressions of the system, performance and concept after the test runs. In particular, they liked the following factors:
    a. The operational procedure was simple
    b. The LED was simple to understand
    c. The automatic system seemed to be working
    d. If the system could function continuously, it would provide significant help to the blower operations
3. The following are the areas that need improvement:
    a. The continuous automatic control should be able to maintain speeds as low as 0.3 m/s
    b. The system should improve its ability to automatically compensate for the combination of the following extreme operational conditions: heavy wet snow, large crab angle, sharp curve, and large super-elevations. Currently, a slight increase in tracking error (up to 4-5 cm) can be observed.
    c. The operator would like to have the option to select different distance from the guardrail for automation for certain operational scenarios.
    d. The system should allow for some negative crab angle for certain special operations, e.g., the case when the operator uses it to compensate for a large snow cut on a sharp curve. Currently the system automatically extends the tracking distance to the guardrail when such a condition is detected to prevent the back end of the snowblower from hitting the guardrail.

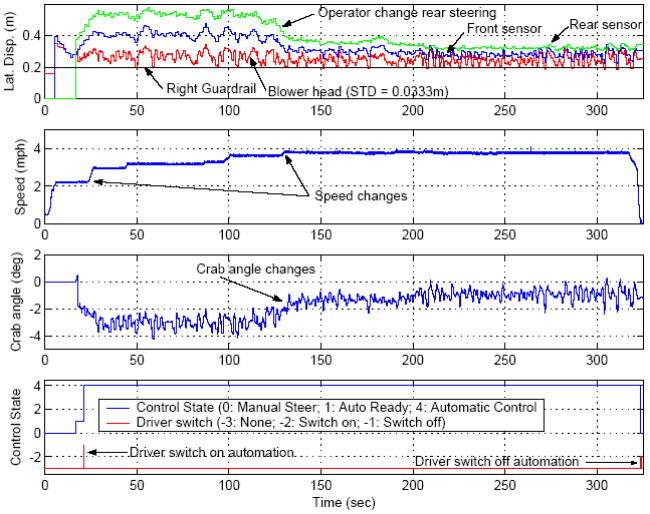

Fig. 10. Snowblower test along guardrail on I-80 (Right Guardrail #1, 02-03-05) - No snow on the ground.

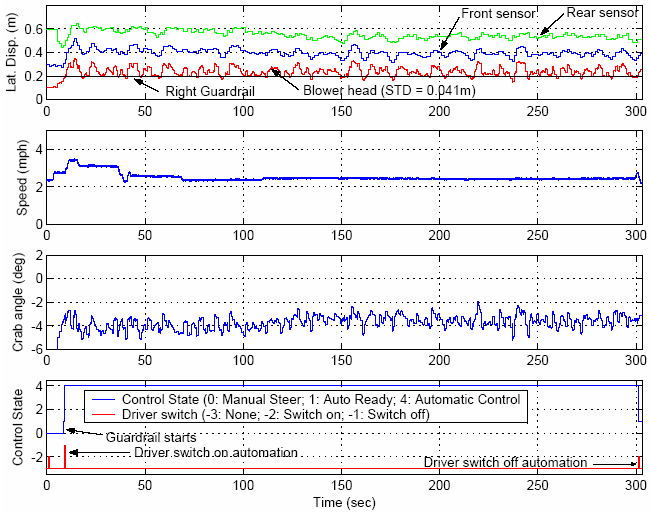

Fig. 11. Snowblower test along guardrail on I-80 (Right Guardrail #1, 03-22-05) - Heavy wet snow on the ground.

As an anecdotal example, in the questionnaires the operators filled out after the trial, they responded to the question:

> *Having seen the automated system, did your opinion on how valuable it could be for snow blowing operations change? Please indicate what your opinion was before and after seeing the system work.*

Driver 1: "Yes – opinion before: a waste of time and money, opinion after: system works, helpful to driver"

Driver 2: "Could be an asset in poor visibility, definitely cut down guardrail damage."

VII. Conclusion

This paper describes a real-world application of lane guidance technologies, which involves the modeling, design, implementation and field testing of an automated snowblower for highway operation along guardrails. The main project objective was to minimize damage to the snowblower, guardrail, and other elements of the infrastructure by deploying highly accurate and robust automated steering. The design difficulties stem from keeping a tight tolerance under all practical operational scenarios and under very stringent conditions: uneven road surface, snow chain effects, variable front tire normal load, large and variable snow removal forces, driver rear steering inputs, and possible operator interventions. This paper presents several critical tasks for this project: problem formulation that explains the design difficulties and defines the system requirements; a new low-speed vehicle model that reveals the source of the low-speed oscillation problem; a low-order controller generated by the understanding of the control problem and validated and refined through the LMI optimization synthesis; a prototype system development that includes hardware, software and HMI installed in the snowblower; and field tests that report successful winter field tests and positive operator responses. This paper does not discuss deployment issues such as maintainability, cost effectiveness, reliability, and commercialization feasibility; nor does it focuses on specific sensor technology selection. Detailed human factor studies and adaptation of GPS-related sensing systems to the snow removal operations are left for possible future work.

Appendix A Enhanced Bicycle Model

The equations of vehicle lateral motion can be derived through the Newtonian method with the assumptions of small steering angles and constant vehicle speed v_r:

$$\begin{aligned} M\ddot{y}_s &= F_{lat}^f + F_{lat}^r - Mv_r^2\rho + F_d \\ I\ddot{\varepsilon}_s &= F_{lat}^f l_1 - F_{lat}^r l_2 + M_{yaw}^f + M_{yaw}^r + M_d \end{aligned} \tag{6}$$

where M is the vehicle mass, and I is the vehicle yaw moment of inertia. In the following derivations, the superscript f and r indicate front wheels and rear wheels, respectively. $F_{lat}^{f/r}$ is the lateral force generated by the tires; and $M_{yaw}^{f/r}$ is the torques introduced by the torsion deformations of the tires about yaw axis. l_1 (l_2) is the distance between the vehicle CG and the front (rear) axle.

In the conventional bicycle model, $F_{lat}^{f/r}$ is proportional to the tire lateral deformations (side slip angles), and $M_{yaw}^{f/r}$ is neglected ($M_{yaw}^f = M_{yaw}^r = 0$). This paper adopts the Dynamic Deflection Tire (DDT) model in [11]. The DDT model assumes tire deformations are generated around tire's three principle axes, i.e. lateral, longitudinal and yaw, with the corresponding tire deflections, σ_y, σ_x and α_{yaw}, being defined as the wheel displacements with respect to the tire contact patch along the three principal axes of the wheel (Fig. 12).

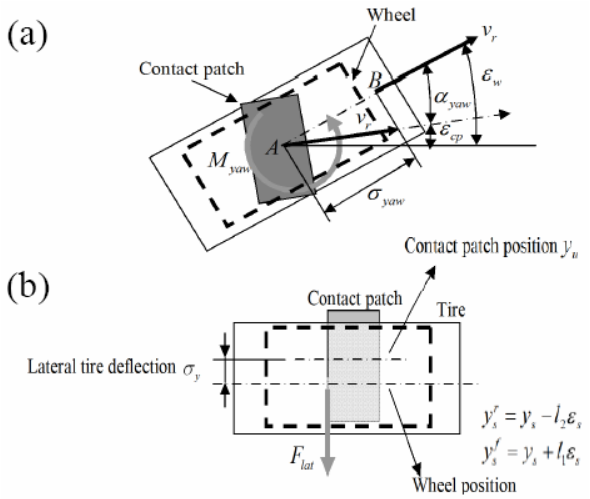

Fig. 12. (a) Yaw deflection & moments; (b) Lateral deflection & forces.

Only σ_y and α_{yaw} are relevant for the lateral dynamics. As shown in Fig. 12, these tire deflections can be defined as:

$$\begin{aligned} &\sigma_y^f = y_s^f - y_u^f \qquad \sigma_y^r = y_s^r - y_u^r \\ &\alpha_{yaw}^f = \varepsilon_w^f - \varepsilon_{cp}^f \qquad \alpha_{yaw}^r = \varepsilon_w^r - \varepsilon_{cp}^r \\ &\varepsilon_w^f = \delta_f + \varepsilon_s + \varepsilon_d \qquad \varepsilon_w^r = \delta_r + \varepsilon_s + \varepsilon_d \end{aligned} \tag{7}$$

where $y_u^{f/r}$ is the tire contact patch positions with respect to the road reference frame; $y_s^f = y_s + l_1\varepsilon_s$ and $y_s^r = y_s - l_2\varepsilon_s$ are the front and rear wheel positions with respect to the road reference frame, respectively; $\varepsilon_w^{f/r}$ is the wheel angle; $\varepsilon_{cp}^{f/r}$ is the tire contact patch angle; and ε_d represents the yaw angle of road reference frame with respect to the inertia frame. One can include the tire damping effect in the DDT model:

$$F_{lat} = D_{lat}\dot{\sigma}_y + C_{lat}\sigma_y \tag{8}$$

$$M_{yaw} = D_{yaw}\dot{\alpha}_{yaw} + C_{yaw}\alpha_{yaw} \tag{9}$$

where D_{lat} and D_{yaw} are the tire lateral and yaw damping coefficients, and C_{lat} and C_{yaw} are the tire lateral and yaw spring constants, respectively. Since the tire tread is continuous and the tire tread within contact patch is in contact with the ground without sliding, the tire contact patch motion is always lagging behind the vehicle body motion. The kinematics of the wheels and contact patch motion can be described as follows:

$$\dot{\varepsilon}_{cp} = v_r(\varepsilon_w - \varepsilon_{cp})/\sigma_{yaw} \tag{10}$$

where σ_{yaw} is the yaw relaxation length. By defining the effective steering angle as $\delta_{eff} = \varepsilon_{cp} - \varepsilon_s - \varepsilon_d$, we have:

$$\dot{\delta}_{eff} = v_r(\delta - \delta_{eff})/\sigma_{yaw} \tag{11}$$

Experimental observation also shows that the effect of rear tire torsion mode is insignificant. Rear wheel steering is also not operated continuously as the front wheel. It is thus reasonable to assume $\dot{\delta}_{eff}^r = 0$. Therefore, $\delta_r = \delta_{eff}^r$, $\varepsilon_{cp}^r = \varepsilon_w^r$ and $M_{yaw}^r = 0$. Similar relations can also be obtained for the lateral contact patch motions as:

$$\begin{aligned} \dot{y}_u^f &= v_r(\delta_{eff}^f + \varepsilon_s) + v_r(y_s^f - y_u^f)/\sigma_{lat} \\ \dot{y}_u^r &= v_r(\delta_r + \varepsilon_s) + v_r(y_s^r - y_u^r)/\sigma_{lat} \end{aligned} \tag{12}$$

where σ_{lat} is lateral relaxation length. By defining the following coordinate transformation and using its derivatives:

$$\begin{aligned} y_u &= (l_1 y_u^r + l_2 y_u^f)/(l_1 + l_2) \\ \varepsilon_u &= (y_u^f - y_u^r)/(l_1 + l_2) \end{aligned}, \quad (13)$$

Eqs. (8-9) can be expressed as:

$$F_{lat}^f = -2D_{lat}^f[\dot{y}_s - \dot{y}_u + l_1(\dot{\varepsilon}_s - \dot{\varepsilon}_u)] - 2C_{lat}^f[y_s - y_u + l_1(\varepsilon_s - \varepsilon_u)]$$

$$F_{lat}^r = -2D_{lat}^r[\dot{y}_s - \dot{y}_u - l_2(\dot{\varepsilon}_s - \dot{\varepsilon}_u)] - 2C_{lat}^r[y_s - y_u - l_2(\varepsilon_s - \varepsilon_u)]$$

$$M_{yaw}^f = -c_2(\dot{\delta}_f - \dot{\delta}_{eff}^f) - k_2(\delta_f - \delta_{eff}^f)$$

$$M_{yaw}^r = 0$$

where $c_2 = 2D_{yaw}^f$ and $k_2 = 2C_{yaw}^f$. Since the data shows that the damping effect of c_2 is small; it is thus reasonable to also assume that $c_2 = 0$. A 7th order state representation of snowblower lateral dynamics is then obtained as in Eq. (1).

REFERENCES

[1] H.-S. Tan, "An Automated Snowblower for Highway Winter Operation," *Intellimotion*, vol. 10, no. 4, pp. 1-6, 2004.

[2] A. Broggi, M. Bertozzi, A. Fascioli, C. Guarino Lo Bianco and A. Piazzi, "The ARGO Autonomous Vehicle's Vision and Control Systems," *International Journal of Intelligent Control Systems*, vol. 3, no. 4, pp. 409-441, 1999.

[3] Q. T. Luong, J. Weber, D. Koller, and J. Malik, "An Integrated Stereo-Based Approach to Automatic Vehicle Guidance," *Proceedings of the 5th ICCV*, pp. 52-57, 1995.

[4] "Validation Report, Intelligent Vehicle Initiative, Specialty Vehicle Field Operational Test", *MN/DOT – US DOT Cooperative Agreement DTFH61-99-X-00101*, July 2002.

[5] J. Farrell, H.-S. Tan and Y. Yang, "Carrier Phase GPS-aided INS based Vehicle Lateral Control". *ASME Journal of Dynamics Systems, Measurement, and Control,* vol. 125, no. 3, pp339-353, 2003.

[6] Lee Alexander, Max Donath. "Differential GPS Based Control of Heavy Vehicles". *Proceedings of the IEEE/IEEJ/JSAI International Conference on Intelligent Transportation Systems,* Tokyo, Japan, pp. 662-7, October, 1999.

[7] H.-S. Tan, B. Bougler and W.-B. Zhang, "Automatic Steering Based on Roadway Markers - From Highway Driving to Precision Docking," *Vehicle System Dynamics*, vol. 37, no. 5, pp. 315-339, 2002.

[8] K. Aoki, T. Suyama, "A concept of intelligent multi-mode transit system based on automated bus" *IEEE Intelligent Vehicles Symposium* 2000, pp. 590 – 595

[9] H.-S. Tan, B. Bougler, and A. Steinfeld, "Snowplow Steering Guidance with Gain Stabilization," *Vehicle System Dynamics*, vol. 36, no. 4-5, pp. 279-305, 2001.

[10] H.-S. Tan, J. Guldner, S. Patwardhan, C. Chen and B. Bougler, "Development of an Automated Steering Vehicle Based on Roadway Magnets - A Case Study of Mechatronic System Design," *IEEE/ASME Transactions on Mechatronics*, vol. 4, no. 3, pp. 258-272, 1999.

[11] S.-L. Koo, H.-S. Tan, "Dynamic-deflection tire modeling for low-speed vehicle lateral dynamics", to appear *ASME Journal of Dynamic Systems, Measurements, and Control*, 2007.

[12] C. Scherer, P. Gahinet and M. Chilali, "Multiobjective Output-Feedback Control Via LMI Optimization," *IEEE Transactions on Automatic Control* , vol. 42, no. 7, pp.896-911, 1997.

[13] S. Boyd, L. El Ghaoui, E. Feron, and V. Balakrishnan, *Linear Matrix Inequalities in Systems and Control Theory.* Philadelphia, PA: SIAM, 1994.

[14] P. Gahinet, A. Nemirovski, A. J. Laub, and M. Chilali, *LMI Control Toolbox for Use with MATLAB*, The Mathworks Inc., 1995.